The Visual Orbit of 64 Piscum

A.F. Boden[1,2], B.F. Lane[5], M.J. Creech-Eakman[5], M.M. Colavita[1], P.J. Dumont[1], J. Gubler[3], C.D. Koresko[5], M.J. Kuchner[4], S.R. Kulkarni[4,5], D.W. Mobley[1], X.P. Pan[4], M. Shao[1], G.T. van Belle[1], J.K. Wallace[1]

(The PTI Collaboration),

B.R. Oppenheimer[4]

Received _____; accepted _____

[1]Jet Propulsion Laboratory, California Institute of Technology

[2]Infrared Processing and Analysis Center, California Institute of Technology

[3]University of California, San Diego

[4]Palomar Observatory, California Institute of Technology

[5]Geology and Planetary Sciences, California Inststute of Technology

ABSTRACT

We report on the determination of the visual orbit of the double-lined spectroscopic binary system 64 Piscum with data obtained by the Palomar Testbed Interferometer in 1997 and 1998. 64 Psc is a nearly equal-mass double-lined binary system whose spectroscopic orbit is well known. We have estimated the visual orbit of 64 Psc from our interferometric visibility data. Our 64 Psc orbit is in good agreement with the spectroscopic results, and the physical parameters implied by a combined fit to our interferometric visibility data and radial velocity data of Duquennoy and Mayor result in precise component masses that agree well with their spectral type identifications. In particular, the orbital parallax of the system is determined to be 43.29 $\pm$ 0.46 mas, and masses of the two components are determined to be 1.223 $\pm$ 0.021 $M_{\odot}$ and 1.170 $\pm$ 0.018 $M_{\odot}$, respectively.

Nadal et al. put forward arguments of temporal variability in some of the orbital elements of 64 Psc, presumably explained by an undetected component in the system. While our visibility data does not favor the Nadal temporal variability inference, neither is it definitive in excluding it. Consequently we have performed both high dynamic-range near-infrared imaging and spectroscopy of potential additional companions to the 64 Psc system. Our imaging and spectroscopic data do not support the conjecture of an additional component to 64 Psc, but we did identify a faint object with unusual red colors and spectra.

1. Introduction

64 Piscum (HD 4676) is a nearby, short-period (13.8 d) binary system with nearly-equal mass ($q \sim 0.96$) components of spectral type F8 V. Further, the 64 Psc binary is the bright component in an apparent visual triple system (Washington Double Star Catalog – WDS, Worley & Douglass 1997). The WDS lists two additional visual components B and C with V of 12.6 and 13.0 at 77 and 71 arcsec separations from 64 Psc, respectively. If these objects are in fact bound to 64 Psc, with a system distance of approximately 24 pc as determined by Hipparcos (ESA 1997, Perryman et al. 1997), the minimum physical separations of the dim B and C components to 64 Psc are approximately 1800 AU, indicating orbital periods of $\sim 5 \times 10^4$ yr.

Abt and Levy (1976, herein AL76) determined the first double-lined spectroscopic orbit for the 64 Psc system. Both Nadal et al (1979, herein N79) and later Duquennoy and Mayor (data in 1991a – herein DM91a, and solution in 1991b – herein DM91b) have determined additional double-lined orbital solutions for the 64 Psc system, which are all in reasonable agreement with each other. Particularly notable is Nadal's argument for the potential presence of an additional, undetected object in the 64 Psc system from possible time variation in the system velocity, the time of periastron passage, and the argument of periastron. N79 used 1918 data from Lick and Mt. Wilson, reanalyzed the AL76 observations, and presented their own data in support of the variation hypothesis. Presumably these time-variation effects could not be due to either the B or C visual companions listed in the WDS; N79 estimates the period of these effects to be $\sim$ 2700 yr.

Herein we report the determination of the 64 Psc visual orbit from near-infrared, long-baseline interferometric measurements taken with the Palomar Testbed Interferometer. PTI is a 110-m K-band (2.2 μm) interferometer located at Palomar Observatory, and described in detail elsewhere (Colavita et al. 1999a). PTI has a minimum fringe spacing of roughly 4 mas at the sky position of 64 Psc, making this binary system readily resolvable.

2. Observations

The interferometric observable used for these measurements is the fringe contrast or *visibility* (squared) of an observed brightness distribution on the sky. Normalized in the interval [0:1], a single star exhibits visibility modulus in a uniform disk model given by:

$$V = \frac{2\,J_1(\pi B\theta/\lambda)}{\pi B\theta/\lambda} \tag{1}$$

where J_1 is the first-order Bessel function, B is the projected baseline vector magnitude at the star position, θ is the apparent angular diameter of the star, and λ is the center-band wavelength of the interferometric observation. The expected squared visibility in a narrow pass-band for a binary star such as 64 Psc is given by:

$$V^2 = \frac{V_1^2 + V_2^2\,r^2 + 2\,V_1\,V_2\,r\,\cos(\frac{2\pi}{\lambda}\,\mathbf{B}\cdot\mathbf{s})}{(1+r)^2} \tag{2}$$

where V_1 and V_2 are the visibility moduli for the two stars separately as given by Eq. 1, r is the apparent brightness ratio between the primary and companion, **B** is the projected baseline vector at the system sky position, and **s** is the primary-secondary angular separation vector on the plane of the sky (Pan et al. 1990, Hummel et al. 1995). The V^2 observables used in our 64 Psc study are both narrow-band V^2 from individual spectral channels (Colavita et al. 1999a), and a synthetic wide-band V^2, given by an incoherent SNR-weighted average V^2 of the narrow-band channels in the PTI spectrometer (Colavita 1999b). In this model the expected wide-band V^2 observable is approximately given by an average of the narrow-band formula over the finite pass-band of the spectrometer:

$$V^2_{wb} = \frac{1}{n}\sum_i^n V^2_{nb-i}(\lambda_i) \tag{3}$$

where the sum runs over the channels covering the infrared K-band (2 - 2.4 μm) of the PTI spectrometer (Colavita et al. 1999a). Separate calibrations and hypothesis fits to the narrow-band and synthetic wide-band V^2 datasets yield statistically consistent results, with the synthetic wide-band data exhibiting superior fit performance. Consequently we will present only the results from the synthetic wide-band data.

Object Name	Spectral Type	Star Magnitude	64 Psc Separation	Adopted Model Diameter (mas)
HD 166	K0 V	6.1 V/4.1 K	16°	0.66 ± 0.06
HD 3651	K0 V	5.9 V/3.9 K	4.9°	0.79 ± 0.05
HD 4628	K2 V	5.7 V/3.5 K	12°	0.92 ± 0.05

Table 1: PTI 64 Psc Calibration Objects Considered in our Analysis. The relevant parameters for our two calibration objects are summarized. The apparent diameter values are determined from effective temperature and bolometric flux estimates based on archival broad-band photometry, and visibility measurements with PTI.

64 Psc was observed in conjunction with our selected calibrator list by PTI on 21 nights between 30 Aug 1997 and 16 Nov 1998, covering roughly 32 periods of the system. 64 Psc, along with calibration objects, was observed multiple times during each of these nights, and each observation, or scan, was approximately 120 sec long. For each scan we computed a mean V^2 value from the scan data, and the error in the V^2 estimate from the RMS internal scatter (Colavita 1999b). 64 Psc was always observed in combination with one or more calibration sources within $\sim$ 20 degrees on the sky. For our study we have used three late-type main sequence stars as calibration objects: HD 166, HD 3651, and HD 4628. Table 1 lists the relevant physical parameters for the calibration objects.

The calibration of 64 Psc V^2 data is performed by estimating the interferometer system visibility (V^2_{sys}) using calibration sources with model angular diameters, and then normalizing the raw 64 Psc visibility by V^2_{sys} to estimate the V^2 measured by an ideal interferometer at that epoch (Mozurkewich et al. 1991, Boden et al. 1998). Calibrating our 64 Psc dataset with respect to the three calibration objects listed in Table 1 results in a total of 88 calibrated scans on 64 Psc over 21 nights in 1997 and 1998.

3. Orbit Determination

The estimation of the 64 Psc visual orbit is made by fitting a Keplarian orbit model with visibilities predicted by Eqs. 2 and 3 directly to the calibrated (narrow-band and synthetic wide-band) V^2 data on 64 Psc (see Armstrong et al. 1992b, Hummel 1993, Hummel et al. 1995, Boden et al. 1999). The fit is non-linear in the Keplarian orbital elements, and is therefore performed by non-linear least-squares methods (i.e. the Marquardt-Levenberg method, Press et al. 1992). As such, this fitting procedure takes an initial estimate of the orbital elements and other parameters (e.g. component angular diameters, brightness ratio), and evolves that model into a new parameter set which best fits the data. However, the chi-squared surface has many local minima in addition to the global minimum corresponding to the true orbit. Because the Marquardt-Levenberg method strictly follows a downhill path in the χ^2 manifold, it is necessary to thoroughly survey the space of possible binary parameters to distinguish between local minima and the true global minimum. In addition, as the V^2 observable for the binary (Eqs. 2 and 3) is invariant under a rotation of 180°, we cannot differentiate between an apparent primary/secondary relative orientation and its mirror image on the sky. Consequently there remains a 180° ambiguity in our determination of the longitude of the ascending node, Ω, which we quote by convention in the interval [0:180). By similar arguments our V^2 observable does not distinguish the longitude of periastron (ω) for the primary and secondary component. We have quoted our estimate constrained to be grossly (within 180°) consistent with the consensus ω_1 value of approximately 200° (AL76, N79, DM91b).

In addition to our PTI visibility data we have used the double-lined radial velocity data from DM91a. To incorporate this data we have upgraded our orbit estimation software to utilize both interferometric visibility and radial velocity data either separately or simultaneously (see similar remarks in Hummel et al. 1998). The ω-degeneracy discussed above is resolved by the inclusion of radial velocity data in our orbital solution (Table 3), however the determination of Ω remains ambiguous by 180°.

In the case of 64 Psc the parameter space is significantly narrowed by the high-quality spectroscopic orbit from both N79 and DM91b, and the Hipparcos distance determination sets

the rough scale of the semi-major axis (ESA 1997). Further, because the 64 Psc system is nearly equal-mass ($q = 0.959 \pm 0.004$ - DM91b), and because interferometric V^2 measurements are only weakly sensitive to variations in intensity ratio near equal intensity, we have constrained the intensity ratios in our fits to 0.90 ($\Delta K = 0.11$) as indicated by our component mass solutions (§4), and the empirical mass-luminosity relationship of Henry and McCarthy (1992). Finally, at the distance of 64 Psc the apparent diameters of the two main-sequence components of the system are not strongly resolved by PTI, so we have constrained the estimated diameters of both components, to 0.5 mas for the primary component and 0.45 mas for the secondary component, as indicated by our system distance and component mass estimates (§4), and a fit to empirical mass-radius data for main sequence eclipsing systems given in Andersen (1991). Given this limited parameter space, the correct orbit solution is readily obtained by exhaustive search.

Figure 1 depicts the relative visual orbit of the 64 Psc system, with the primary component rendered at the origin, and the secondary component rendered at periastron. We have indicated the phase coverage of our V^2 data on the relative orbit with heavy lines; our data samples most phases of the orbit well, leading to a reliable orbit determination.

Table 2 lists the complete set of V^2 measurements in our 64 Psc dataset and the prediction based on the best-fit orbit model (our full-fit model, Table 3) for 64 Psc. Table 2 gives V^2 measurements and times, measurement errors, model predictions, the photon-weighted average wavelength, $u - v$ coordinates, and on-target hour angle for each of our calibrated 64 Psc observations. Figure 2a shows four consecutive nights of PTI V^2 data on 64 Psc (30 Aug – 2 Sept 1997), and V^2 predictions based on the best-fit model for the system (our full-fit model, Table 3). The model predictions are in good agreement with the observed data, with an RMS V^2 residual of 0.034 (average absolute V^2 deviation of 0.053), and a χ^2 per Degree of Freedom (DOF) of 0.85. Figure 2b gives a radial velocity phase plot of the DM91a radial velocity data and the predictions of our full-fit orbital solution. A radial velocity fit residual histogram is also included.

Spectroscopic orbit parameters (from N79 and DM91b) and our visual and spectroscopic

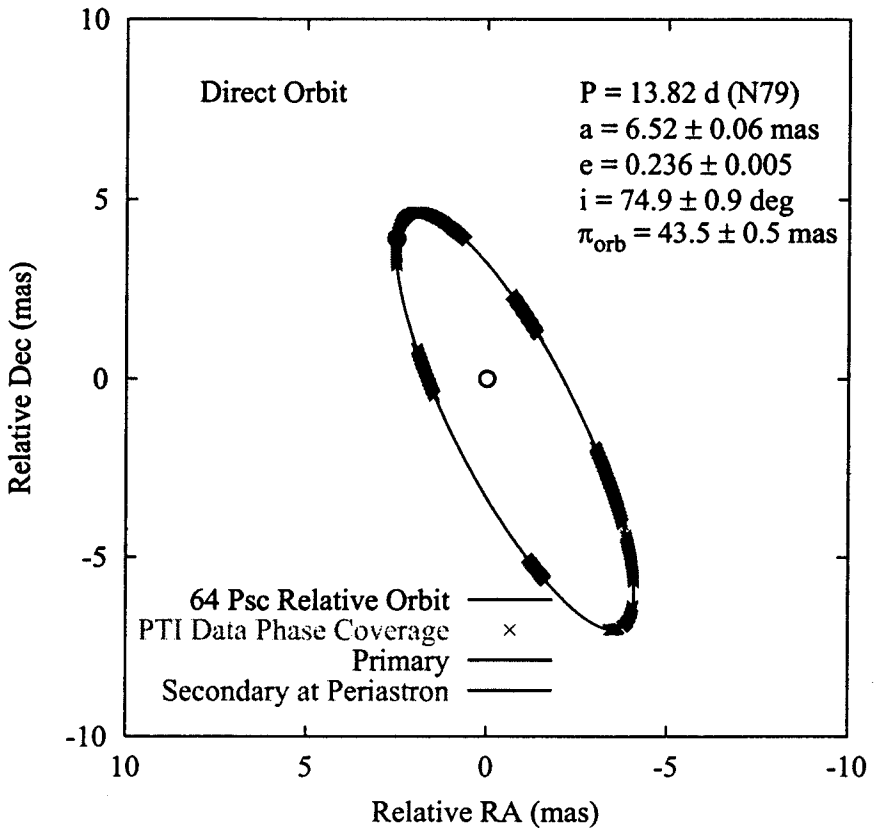

Fig. 1.— Visual Orbit of 64 Psc. The relative visual orbit of 64 Psc is shown, with the primary and secondary objects rendered at T_0 (periastron). The heavy lines along the relative orbit indicate areas where we have orbital phase coverage in our PTI data (they are not separation vector estimates); our data samples most phases of the orbit well, leading to a reliable orbit determination.

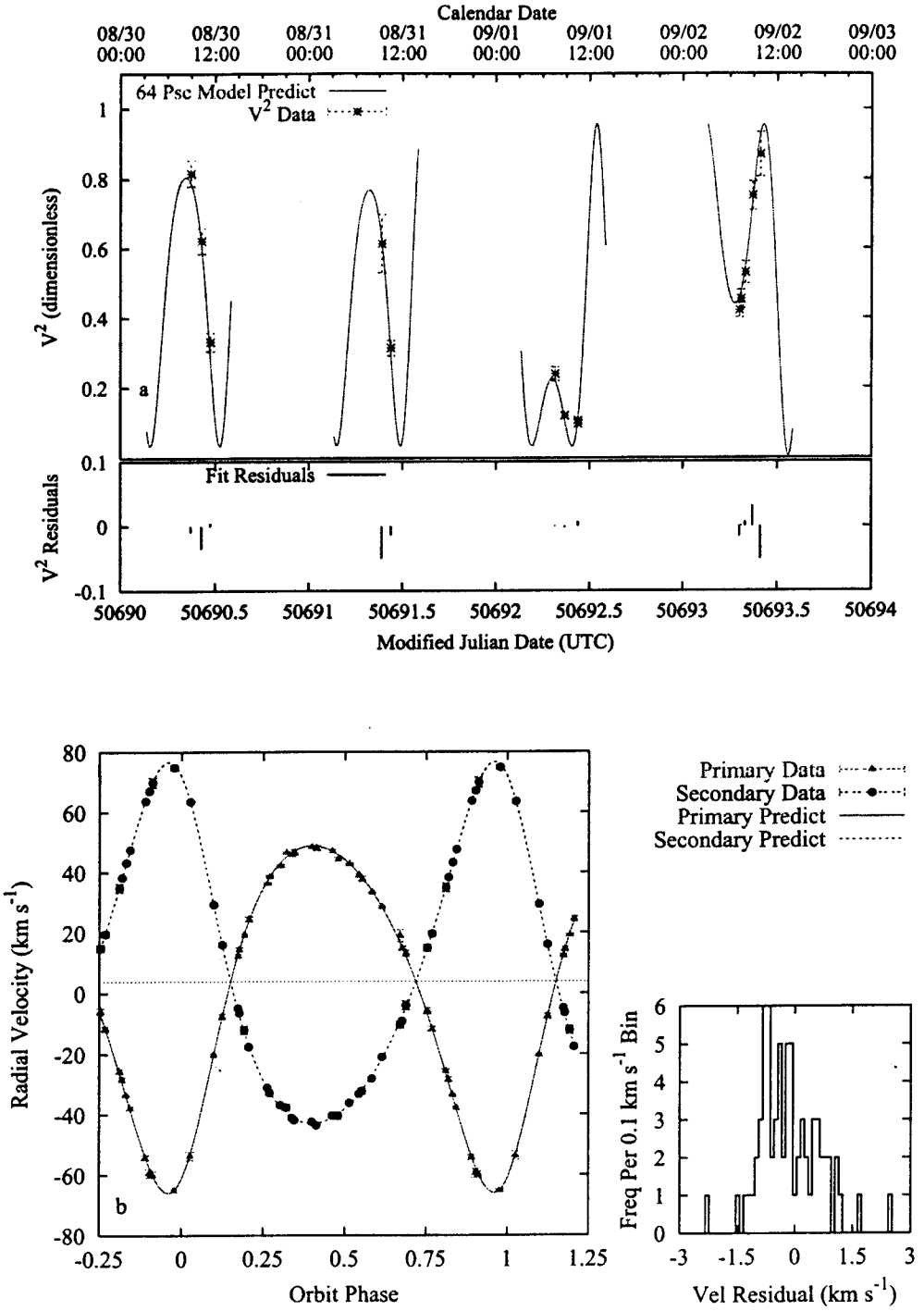

Fig. 2.— V^2 and RV Fit of 64 Psc. a: Four consecutive nights (30 Aug – 2 Sept 1997) of calibrated V^2 data on 64 Psc, and V^2 predictions from the best-fit model for the system. The lower frame shows individual V^2 residuals between the calibrated data and best-fit model. b: A phase plot of radial velocity data from DM91a and fit predictions from our Full-Fit solution (Table 3). Also included is a histogram of RV residuals around the double-lined solution.

orbit parameters of the 64 Psc system are summarized in Table 3. We give the results of separate fits to only our V^2 data (our V^2-only Fit solution), and a simultaneous fit to our V^2 data and the double-lined radial velocities from DM91a (our Full-Fit solution) – both with relative intensity and component diameters constrained as noted above. For the orbit parameters we have estimated from our visibility data we list a total one-sigma error in the parameter estimate, and the separate one-sigma errors in the parameter estimates from statistical (measurement uncertainty) and systematic error sources. In our analysis the dominant forms of systematic error are: (1) uncertainties in the calibrator angular diameters (Table 1); (2) uncertainty in our center-band operating wavelength ($\lambda_0 \approx 2.2$ μm), which we have taken to be 20 nm ($\sim$1%); (3) the geometrical uncertainty in our interferometric baseline ($< 0.01\%$); and (4) uncertainties in orbital parameters we have constrained in our fitting procedure (i.e. the component intensity ratio and angular diameters in both solutions). Different parameters are affected differently by these error sources; e.g. our estimated uncertainty in the 64 Psc orbital inclination is dominated by measurement uncertainty, while the uncertainty in the angular semi-major axis is dominated by uncertainty in the wavelength scale. Conversely, we have assumed that all of the error quoted by N79 and DM91b in the 64 Psc spectroscopic parameters is statistical.

There is a significant ($\sim$ 4.2-sigma) difference in the period as estimated by DM91b and the period estimates of N79 and PTI. For the full-fit solution our period estimate exploits the roughly 7300-day (530 64 Psc orbital cycles) time baseline between the DM91a RV data and our own visibility data. Both our period estimates agree well with the N79 determination (the full-fit solution agreement with N79 is $\sim$ 0.9-sigma).

4. Physical Parameters

Physical parameters derived from our 64 Psc full-fit visual/spectroscopic orbit are summarized in Table 4. As in Table 3, for physical parameters we have estimated we quote total sigma error, and its statistical and systematic contributions. Notable among these is the high-precision determination of the component masses for the system, a virtue of the precision of the DM91a

Orbital Parameter	N79	DM91b	PTI 97/98	
			V^2-only Fit	Full Fit
Period (d)	13.824581	13.8318	13.82407	13.824621
	$\pm$ 4.0 $\times$ 10^{-5}	$\pm$ 1.7 $\times$ 10^{-3}	$\pm$ 4.4 (3.8/2.2) $\times$ 10^{-4}	$\pm$ 1.7 (1.7/0.4) $\times$ 10^{-5}
T_0 (MJD)	41933.702	43468.308	50905.934	50905.984
	$\pm$ 0.074	$\pm$ 0.018	$\pm$ 0.068 (0.048/0.048)	$\pm$ 0.015 (0.015/0.003)
e	0.243 $\pm$ 0.010	0.238 $\pm$ 0.002	0.2348	0.2376
			$\pm$ 0.0052 (0.0035/0.0039)	$\pm$ 0.0012 (0.0011/0.0005)
K_1 (km s^{-1})	57.53 $\pm$ 0.74	57.31 $\pm$ 0.19		57.35 $\pm$ 0.31 (0.31/0.01)
K_2 (km s^{-1})	58.77 $\pm$ 0.75	59.77 $\pm$ 0.18		59.95 $\pm$ 0.32 (0.31/0.02)
ω_1 (deg)	199.6 $\pm$ 2.2	202.3 $\pm$ 0.5	202.2 $\pm$ 1.9 (1.3/1.3)	203.56 $\pm$ 0.35 (0.33/0.10)
Ω_1 (deg)			63.43 $\pm$ 0.68 (0.66/0.16)	63.60 $\pm$ 0.82 (0.81/0.16)
i (deg)			74.37 $\pm$ 0.96 (0.92/0.27)	73.80 $\pm$ 0.92 (0.91/0.17)
a (mas)			6.516 $\pm$ 0.061 (0.016/0.059)	6.527 $\pm$ 0.061 (0.015/0.059)
ΔK (mag)			*0.11*	*0.11*
χ^2/DOF			0.85	1.2 (0.95 V^2/2.8 RV)
$\overline{\lvert R_{V^2} \rvert}$			0.053	0.053
$\overline{\lvert R_{RV} \rvert}$ (km s^{-1})		0.65		0.65

Table 3: Orbital Parameters for 64 Psc. Summarized here are the apparent orbital parameters for the 64 Psc system as determined by N79, DM91b, and PTI. We give two separate fits to our data, with and without including the double-lined DM91a radial velocities in the fit (constrained parameters are listed in italics). For parameters we have estimated from including our PTI observations we separately quote one-sigma errors from both statistical and systematic sources, given as $(\sigma_{stat}/\sigma_{sys})$, and the total error as the sum of the two in quadrature. We have quoted the longitude of the ascending node parameter (Ω) as the angle between local East and the orbital line of nodes measured positive in the direction of local North. Due to the degeneracy in our V^2 observable there is a 180° ambiguity in Ω; by convention we quote it in the interval of [0:180). We quote mean absolute V^2 and RV residuals in the fits, $\overline{\lvert R_{V^2} \rvert}$ and $\overline{\lvert R_{RV} \rvert}$ respectively.

radial velocity measurements on both components and the high inclination of the orbit. We estimate the masses of the F8V primary and secondary components as 1.223 ± 0.021 $M_\odot$ and 1.170 ± 0.018 $M_\odot$, respectively. Remarkably, these are very near the values estimated by N79, based on their radial velocities and the relative magnitude in the system.

The Hipparcos catalog lists the parallax of 64 Psc as 41.80 ± 0.75 mas (ESA 1997). The distance determination to 64 Psc based on our orbital solution is 23.10 ± 0.24 pc, corresponding to an orbital parallax of 43.29 ± 0.46 mas, consistent with the Hipparcos result at 3.5% and 1.7-sigma.

Based on eclipsing binary systems, Popper (1980) and Andersen (1991) list main-sequence linear diameters for stars in the mass range of the 64 Psc components at 1.15 – 1.25 $R_\odot$. At a distance of approximately 23 pc this corresponds to apparent angular diameters in the range of 0.42 – 0.5 mas. This range of apparent diameters is unresolved to our interferometer, with expected component visibility moduli (Eq. 1) of approximately 0.99. Consequently, as discussed above we have adopted model diameters for the two components based on a fit to Andersen's compilation of eclipsing binary data in this mass range. In particular we have constrained our solutions to a primary diameter of 0.5 mas (1.24 $R_\odot$ @ 23 pc) and a secondary diameter 0.45 (1.12 $R_\odot$ @ 23 pc) respectively, and included 10% one-sigma errors around these constraints into our systematic error computations. We have also ignored any corrections due to stellar limb darkening; our data would be highly insensitive to these effects.

Similarly, because the system is nearly equal mass, hence nearly equal brightness, our V^2 data is relatively insensitive to the magnitude difference of the two components (see Hummel et al. 1998 for similar comments). Based on our masses and the mass-luminosity models of Henry & McCarthy (1992, 1993) one would expect a K-magnitude difference of 0.11 and a V-magnitude difference of 0.24. For reference, N79 quoted a best-fit component magnitude difference in the visible of 0.16 without a quoted error. An independent fit of our PTI data for a K-band magnitude difference between the two yields components 0.141 ± 0.076 – well within one sigma of the expected K-band magnitude difference. As noted above for our orbit fit we have chosen

to constrain the K-magnitude difference at its model value, and included a 5% one-sigma error around this constraint in our systematic error computations. However, our fit K-band magnitude difference, system distance estimate, and a 64 Psc apparent (CIT) K-band magnitude estimate of 3.88 $\pm$ 0.07 yields K-band absolute magnitude estimates of 2.75 $\pm$ 0.08 and 2.89 $\pm$ 0.09 for the primary and secondary components respectively. These estimates agree well with the predictions of the mass-luminosity model of Henry and McCarthy (Henry & McCarthy 1992), which predicts absolute K-band magnitudes of 2.79 and 2.91 for the primary and secondary components respectively.

5. Temporal Variations in Orbital Elements

N79 argued for the possible presence of an additional, undetected object in the 64 Psc system from supposed temporal variations in the systematic velocity, the time of periastron (T_0), and the argument of (primary) periastron (ω_1). In particular, N79 gives plots of systematic velocity, projected T_0, and ω_1 as a function of observation epoch. Assuming the N79 estimate for the period of the effects (2700 yr), the approximate angular separation between 64 Psc and this third component would be $\sim$ 10 arcsec, sufficiently distant to not affect our V^2 measurements on the inner pair, and thus not perturb our orbit reconstruction.

Our interferometric data does not address the 64 Psc systematic velocity, but we can test the consistency of the N79 orbital element trends with our orbit solution. Because we note a bias in the period estimate could produce the linear effects in projected T_0 that N79 claims, the comparison is best done with ω_1. Figure 3 gives a plot of various values of ω_1 as reported by AL76, N79, DM91b, and PTI. Updating the N79 model for ω_1, we have fit a linear model to ω_1 based on 1918 measurements made at Lick and Mt. Wilson (reduced by N79), AL76 (reanalyzed by N79), N79 themselves, and DM91b. As depicted in Figure 3, this model is dominated by the estimate determined by N79 from the 1918 Lick/Wilson data, and based on the errors quoted by N79 the data will support a broad range of trends for the time-variation of ω_1 – including essentially no variation. The updated N79 model for ω_1 evaluated at the epoch of our 1997/1998

PTI observations is not in particularly good agreement with our V^2-fit and full-fit values for ω_1 of 202.7 $\pm$ 1.9 and 203.56 $\pm$ 0.35 respectively (Table 3); it predicts a value for ω_1 of 205.0 $\pm$ 2.0 deg. Shown in Figure 3, the disagreement (4-sigma) of our full-fit ω_1 determination to this linear model central projection would seem to cast doubt on the evolving-ω_1 hypothesis at a reasonably high confidence level. The potential problem with drawing a firm conclusion on the evolution question is the inclusion of the older DM91a radial velocities – while the RV data match our recent visibility measurements very well, they may well bias the ω_1 estimate away from its current true value.

6. Companion Search

Because our 64 Psc orbital studies do not rule out the presence of a companion as N79 suggest, we imaged the 64 Psc system with the Near-Infrared Camera (NIRC) on the Keck-I telescope at Mauna Kea on 20 October 1998, and again on 28 November 1998. A panel of near-infrared images of the 64 Psc system is shown in Figure 4.

These images were obtained through the J, H and K filters with total integration times of 60 s – the data from six 10 s exposures being coadded into a memory buffer before being recorded to disk. In the J band we took 10 such images while moving the telescope pointing by 10 pixels between each exposure to limit the effects of bad pixels on the array. These 10 images were then shifted and added. The same procedure was used at H and K band, but only 7 images were taken in H and 1 in K. These were sufficient to detect objects down to $J = 21.0$, $H = 20.2$ and $K = 19.0$, where the total exposure times are 600 s, 420 s and 60 s for J, H and K respectively. Clearly the presence of the bright 64 Psc system in the images makes detecting faint objects difficult. By reflecting the images along the central vertical axis (where the star was positioned) and subtracting this reflected image from the original, a substantial portion of the star light is removed. (See Matthews et al. 1996 for a detailed description of this technique.) This subtracted image is used for photometry of the remaining objects. We used the standard SJ9101 (HST P525-E, Persson et al. 1998) to calibrate the instrumental magnitudes and determine the flux density of the point sources we found in these images.

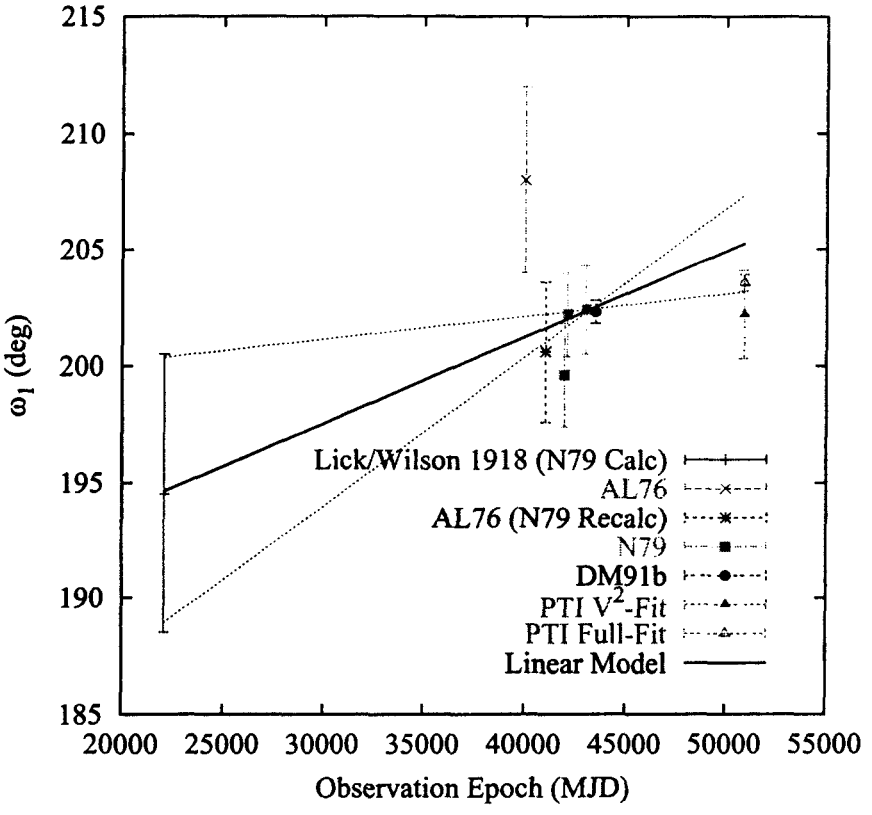

Fig. 3.— Measurements of ω_1 vs. Time for 64 Psc. At least as calculated by N79, measurements of ω_1 vs. epoch of observation show a striking linear trend, and N79 suggest the presence of an additional, undetected body in the 64 Psc system to explain these effects. The N79 linear model for ω_1 (updated here to include the DM91b determination, but not the PTI result) is not in particularly good agreement with the value for ω_1 estimated from our 1997/1998 PTI observations of 64 Psc (both separately and in combination with the DM91a radial velocity measurements). Our combined interferometry-radial velocity determination of ω_1 is sufficiently accurate to formally exclude the N79 evolution hypothesis at high confidence, but it conceivably may be biased by the older radial velocities.

There are two apparent point sources other than 64 Psc itself in our images, which following the WDS conventions we will refer to as 64 Psc D and E (momentarily leaving aside the issue of whether these objects are actually assocated with the 64 Psc system). To determine the offsets of the D and E objects with respect to 64 Psc we had to determine the position of 64 Psc on the detector, which was completely saturated within a radius of 23 pixels of the star. (The pixel scale is 0.15".) The star's position was determined by fitting lines through the unsaturated portions of the 6 diffraction spikes yielding a position with a conservative accuracy of better than 0.05" (a third of a pixel). The first point source, herein 64 Psc D, is in the upper right of the images, separated from 64 Psc by 22.7" at a position angle of 250°, measured N through E. This point source has the following magnitudes: $J = 17.0 \pm 0.1$, $H = 16.8 \pm 0.1$ and $K = 16.6 \pm 0.1$. This photometry is consistent with that of a background G7 V star at a distance of roughly 4 kpc. It is therefore apparently excluded as a possible companion to 64 Psc.

The other point source, herein 64 Psc E, is much dimmer than the D companion, and we have highlighted it in the figures with a red arrow to indicate its position. 64 Psc E is separated from 64 Psc by 12.1" at a PA of 60°, and is extremely red; it is undetected in the J image, but visible in H and clearly detected at K bands. 64 Psc E shows no obvious signs of extended structure in either the H or K- band images. Photometric measurements of 64 Psc E yield the following: $J > 21.0$, $H = 19.3 \pm 0.2$, $K = 18.5 \pm 0.15$. If this candidate is physically associated with 64 Psc it would have an $M_K = 16.7$ making it 2.4 magnitudes fainter than Gliese 229B, the coolest known brown dwarf and the least luminous condensed object directly detected outside the solar system.

Because of 64 Psc Es intriguing red color, and the fact that the separation between it and 64 Psc is so near the calculated separation if the N79 conjecture were correct, we obtained a near-infrared spectrum with NIRC on the night of 28 November 1998.

To obtain the spectrum we used NIRC's 120 line mm^{-1} grism in conjunction with the 4 pixel slit (chosen to match the seeing) and blocking filters which permit only the H and K bands to pass through to the detector. The object was positioned on the slit and 14 exposures of 60 s integration (1 coadd) were taken, while moving the object along the slit by 10 arcseconds between

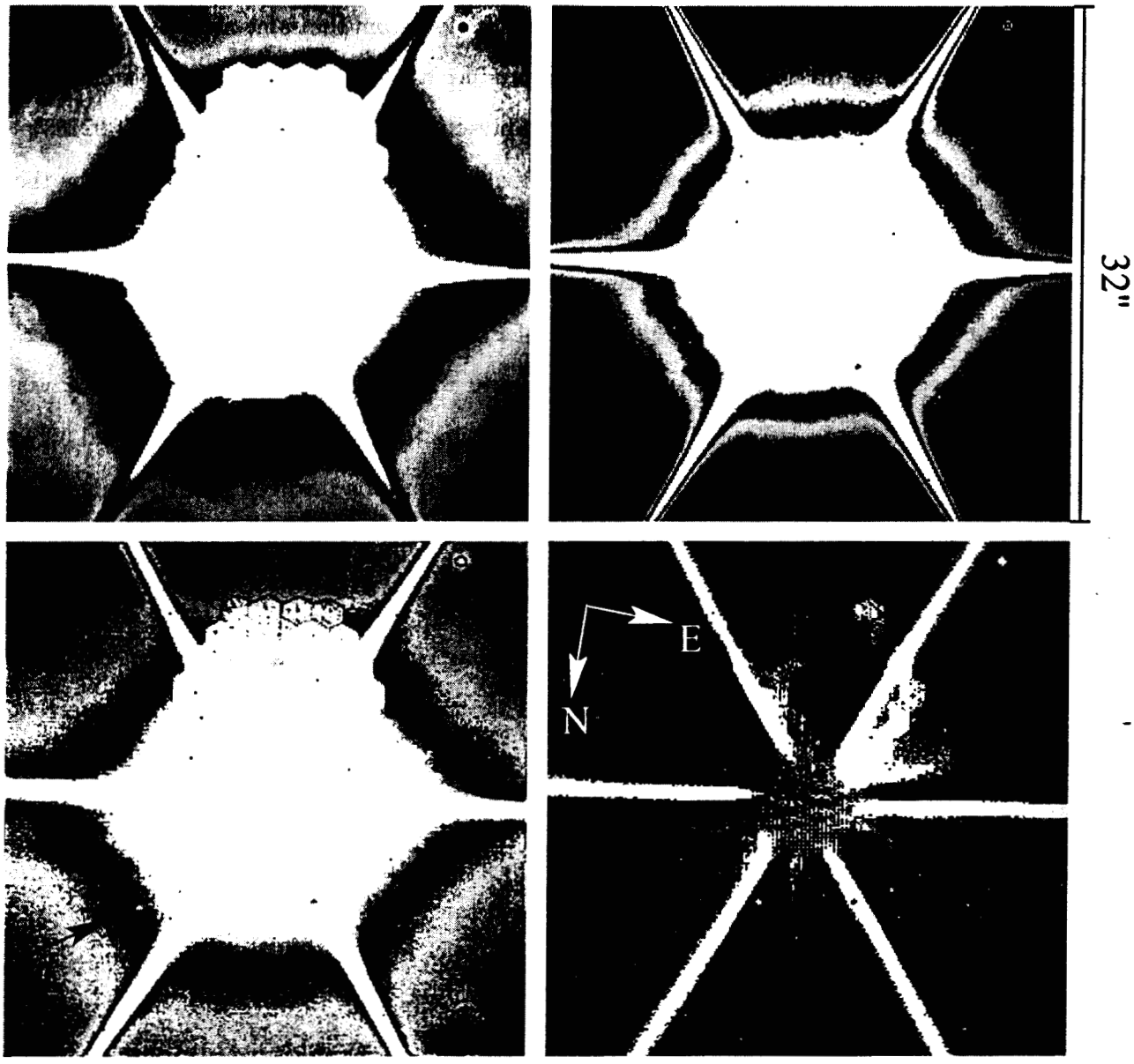

Fig. 4.— Keck NIRC images of 64 Psc. Left-to-Right, Top-to-Bottom the images are J-band (1.2 μm), H-band (1.6 μm), K-band (2.2 μm), and a K minus K-reflected image (see the text for an explanation of this last image). The field of view is $32''$ on a side with a pixel size of $0.15''$. The red arrow indicates the peculiar object, which we call 64 Psc E, whose spectrum is shown in Fig. 5. 64 Psc E's J - K color is $> 2.5^m$.

exposures. This permitted us to extract spectra from every exposure. We then observed the standard G8III star SAO 92183 to provide a spectral flatfield from the same airmass. SAO 92183 was smeared across the entire length of the slit to produce a "flatfield" over the whole detector. A sky frame was taken identically to be used for subtraction from the reference (SAO 92183) spectral image. The data were reduced by summing all the spectral images and dividing by the reference spectral image. Then the spectrum of 64 Psc E and that of one of the diffraction spikes of 64 Psc were extracted separately. The two were separated by 5" in the spectral images. This means that it is unlikely any contamination from 64 Psc is present in the spectrum of 64 Psc E. The spectra were extracted by summing the 7 rows over which the signal from each source was visible. The extracted spectra were then wavelength calibrated using the well-determined 50% transmission points of the HK blocking filter. The flux calibration involved first the removal of the Rayleigh-Jeans falloff of the reference G-star used to flat field the data and a matching of the K-band integrated flux to that measured by the photometry.

The spectra from 1.4 to 2.5 μm of both the candidate companion 64 Psc E and 64 Psc itself are shown in Figure 5. The candidate spectrum is extremely red, confirming the photometric measurements, and it is substanitally different from the composite spectrum of the two late F-star components of 64 Psc. This demonstrates that little or no contamination from 64 Psc itself is present in the spectrum of 64 Psc E. While the SNR is low, there are no apparent molecular features in the spectrum. In particular the large methane features seen in the spectrum of the cool brown dwarf GL 229B (see Oppenheimer et al. 1995, Geballe et al. 1998, Oppenheimer et al. 1998) are notably absent.

Based on the colors and proximity of the first (64 Psc D) candidate, and the implied large absolute magnitude of the second (64 Psc E) candidate, we think it is unlikely that either object is physically associated with the 64 Psc system. However, 64 Psc E is relatively unusual in its extreme red colors. Based on initial statistics from the 2MASS survey, L-dwarfs typically have J - K colors less than 2.1, so that possibility would seem to be unlikely (Kirkpatrick et al. 1999). Other possible explanations for the extreme red nature of 64 Psc E is the possibility of a very red

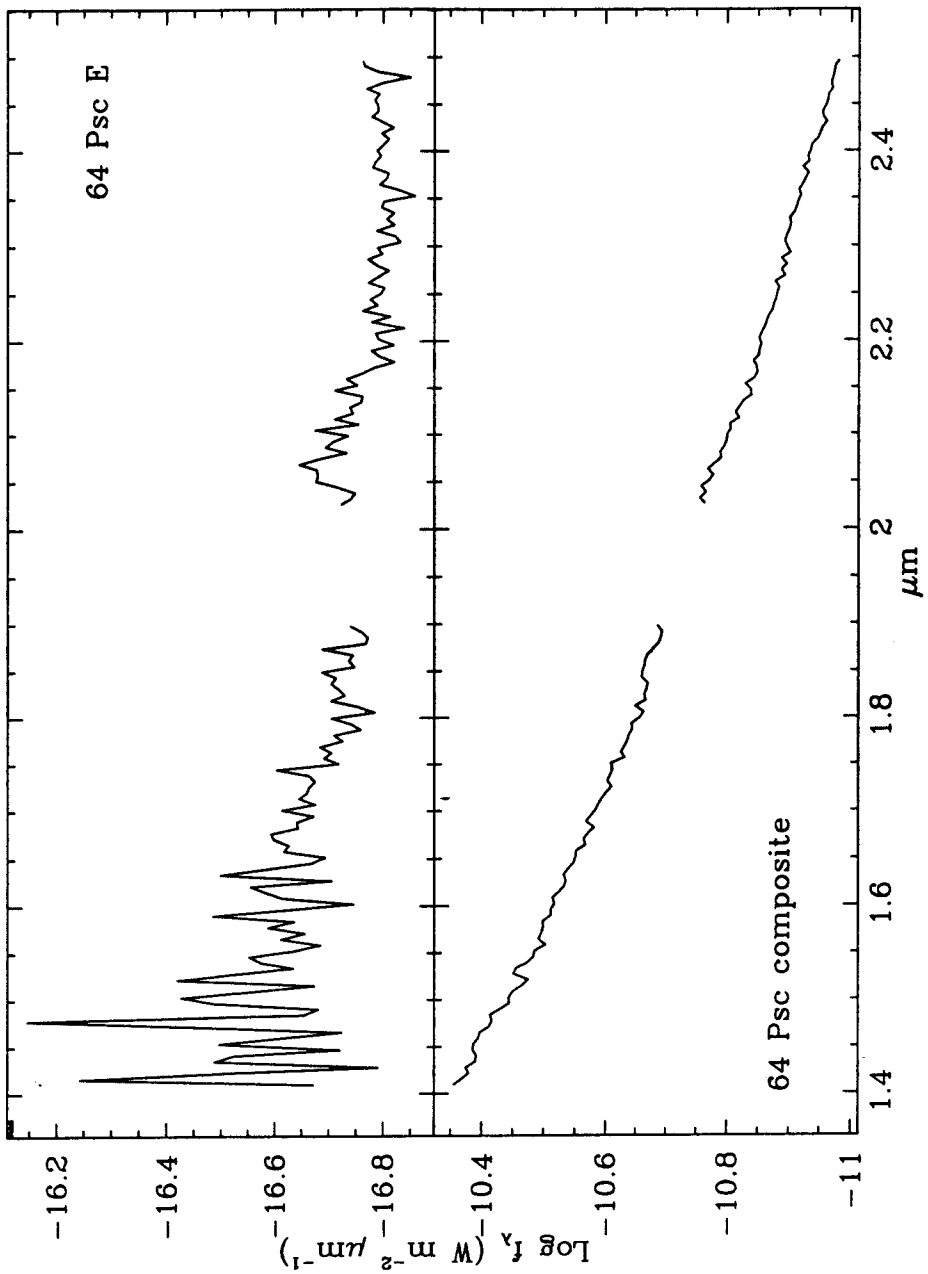

Fig. 5.— The near-infrared spectrum of the candidate companion of 64 Psc, 64 Psc E, is shown in the top panel. The bottom panel is the composite spectrum of the two F stars that comprise 64 Psc. That spectrum was taken from the diffraction spike which passed through the slit of the spectrograph. The gap in both spectra between 1.9 and 2.0 μm is where the atmospheric absorption prevented measurement. We estimate the SNR in the 64 Psc E spectrum is approximately 2 in the blue edge of the H-band and 35 in the red end of the K-band.

QSO (Beichman et al. 1998), or a red, compact background galaxy (Becklin et al. 1995, Graham & Dey 1996, Stanford et al. 1997). It is clearly interesting to determine whether the 64 Psc E object shows indications of common proper motion with 64 Psc itself, and a higher SNR spectrum of the object would be needed to unequivocally establish the nature of 64 Psc E.

7. Summary and Discussion

By virtue of our interferometric resolution and the high precision of the DM91a radial velocity data we are able to determine accurate masses of the 64 Psc constituents, and an accurate system distance. Our data favors the earlier spectroscopic period of N79 over the more recent DM91b determination. The approximate determination of relative K-brightness ratio of the two nearly-equal brightness 64 Psc constituents (best-fit K-magnitude difference of 0.141 $\pm$ 0.076) prevents us from establishing tight constraints on the absolute magnitudes of the components. This is regrettable, but is an inherent limitation of our amplitude-only reconstruction technique for nearly equal-brightness systems (Hummel et al. 1998).

The N79 suggestion of an additional body in the system as an explanation for purported orbital parameter variation is intriguing, but our orbital results do not seem to favor this inference. However, these considerations suggest high angular resolution, high dynamic range imaging of the system to attempt a detection of a companion, and we have imaged the 64 Psc system with NIRC at Keck-I. Neither of the two potential companion candidates apparent in our near-infrared images seem likely to be physically associated with the 64 Psc system. However, the second of these candidates (herein 64 Psc E) would appear to be fairly unusual based on its very red colors and spectrum in the near-infrared, and follow-up proper-motion and spectroscopic observations would be warranted.

The work described in this paper was performed at the Jet Propulsion Laboratory and the Infrared Processing and Analysis Center, California Institute of Technology under contract with the National Aeronautics and Space Administration. Interferometer data was obtained at the

Palomar Observatory using the NASA Palomar Testbed Interferometer, supported by NASA contracts to the Jet Propulsion Laboratory. Imaging and spectroscopic data was obtained at the W.M. Keck Observatory at Mauna Kea, Hawaii, operated by the California Association for Research in Astronomy. We thank K.Y. Matthews (CIT) for assistance with near-infrared photometry on 64 Psc. A.F.B. in particular thanks C.A. Hummel (USNO) for his suggestion concerning integrated fitting of interferometric visibilities and radial velocities.

We wish to thank the anonymous referee for his many positive contributions to the accuracy and quality of this manuscript.

This research has made use of the Simbad database, operated at CDS, Strasbourg, France.

Physical Parameter	Primary Component	Secondary Component
a (10^{-2} AU)	7.371 ± 0.052 (0.052/0.006)	7.706 ± 0.054 (0.054/0.07)
Mass ($M_\odot$)	1.223 ± 0.021 (0.021/0.002)	1.170 ± 0.018 (0.018/0.002)
Sp Type (DM91b)	F8V	F8V
Model Diameter (mas)	0.5 (const)	0.45 (const)
System Distance (pc)	23.10 ± 0.24 (0.13/0.21)	
π_{orb} (mas)	43.29 ± 0.46 (0.24/0.39)	
M_K (mag)	2.75 ± 0.08 (0.07/0.04)	2.89 ± 0.09 (0.08/0.04)

Table 4: Physical Parameters for 64 Psc. Summarized here are the physical parameters for the 64 Psc system as derived from the orbital parameters in Table 3. As for our PTI-derived orbital parameters we have quoted both total error and separate contributions from statistical and systematic sources (given as $\sigma_{stat}/\sigma_{sys}$).

REFERENCES

Abt, H. and Levy, S. 1976 (AL76), ApJS 30, 273.

Andersen, J. 1991, A&A Rev. 3, 91.

Armstrong, J.T. et al. 1992, AJ 104, 2217.

Becklin, E., Macintosh, B., and Zuckerman, B. 1995, ApJ 449, L117.

Beichman, C. et al 1998, PASP 110, 367.

Boden, A.F. et al. 1998, Proc. SPIE 3350, 872.

Boden, A.F. et al. 1999, ApJ 515, 356 (astro-ph/9811029).

Colavita, M.M. et al. 1999a, ApJ 510, 505 (astro-ph/9810262).

Colavita, M. 1999b, PASP 111, 111 (astro-ph/9810462).

Duquennoy, A., and Mayor, M. 1991a (DM91a), A&A 248, 485.

Duquennoy, A., and Mayor, M. 1991b (DM91b), A&A 248, 485.

ESA 1997, The Hipparcos and Tycho Catalogues, ESA SP-1200.

Geballe, T., Kulkarni, S., Woodward, C., and Sloan, G. 1998, ApJ 467, L101.

Graham, J., and Dey, A. 1996, ApJ 471, 720.

Henry, T. and McCarthy, D. 1992, Proc. Comp. Double Star Research, IAU Col. 135, McAlister, H. and Hartkopf, W. ed.

Henry, T. and McCarthy, D. 1993, AJ 106, 773.

Hummel, C.A. et al. 1993, AJ 106, 2486.

Hummel, C. et al. 1995, AJ 110, 376.

Hummel, C. et al. 1998, AJ 116, 2536.

Kickpatrick, D. et al. 1999, ApJ in press (http://www.ipac.caltech.edu/2mass/).

Matthews, K., Nakajima, T., Kulkarni, S., and Oppenheimer, B. 1996, AJ 112, 1678.

Mozurkewich, D. et al. 1991, AJ 101, 2207.

Nadal, R., Ginestet, N., Carquillat, J.M., and Pedoussaut, A. 1979 (N79), A&AS 35, 203.

Oppenheimer, B., Kulkarni, S., Matthews, K., and Nakajima, T. 1995, Science 270, 1478.

Oppenheimer, B., Kulkarni, S., Matthews, K., and van Kerkwijk, M. 1998, ApJ 502, 932.

Pan, X. et al. 1990, ApJ 356, 641.

Perryman, M.A.C. et al. 1997, A&A 323, L49.

Persson, S., Murphy, D., Krezeminski, W., Roth, M., and Rieke, M. 1998, AJ116, 2475.

Popper, D. 1980, ARA&A 18, 115.

Press, W.H., Teukolsky, S.A., Vetterling, W.T., and Flannery, B.P. 1992, Numerical Recipes in C: The Art of Scientific Computing, Second Edition, Cambridge University Press.

Stanford, S. et al. 1997, AJ 114, 2232.

Worley, C. and Douglass, G. 1997, A&AS 125, 523.

This manuscript was prepared with the AAS LaTeX macros v4.0.